BIOCHEMISTRY
including biophysical chemistry & molecular biology
Article

Biochemistry **2009,** *48,* 11883–11891 11883
DOI: 10.1021/bi9016395

Influence of Proline upon the Folding and Geometry of the WALP19 Transmembrane Peptide†

Rachel Thomas, Vitaly V. Vostrikov, Denise V. Greathouse, and Roger E. Koeppe II*

Department of Chemistry and Biochemistry, University of Arkansas, Fayetteville, Arkansas 72701

Received September 18, 2009; Revised Manuscript Received November 4, 2009

ABSTRACT: The orientations, geometries, and lipid interactions of designed transmembrane (TM) peptides have attracted significant experimental and theoretical interest. Because the amino acid proline will introduce a known discontinuity into an α helix, we have sought to measure the extent of helix kinking caused by a single proline within the isolated TM helical domain of WALP19. For this purpose, we synthesized acetyl-GWWLALALA-P[10]ALALALWWA-ethanolamide and included pairs of deuterated alanines by using 60−100% Fmoc-L-Ala-d_4 at selected sequence positions. Solid-state deuterium (^{2}H) magnetic resonance spectra from oriented, hydrated samples (1/40, peptide/lipid; using several lipids) reveal signals from many of the alanine backbone C_α deuterons as well as the alanine side-chain C_β methyl groups, whereas signals from C_α deuterons generally have not been observed for similar peptides without proline. It is conceivable that altered peptide dynamics may be responsible for the apparent "unmasking" of the backbone resonances in the presence of the proline. Data analysis using the geometric analysis of labeled alanines (GALA) method reveals that the peptide helix is distorted due to the presence of the proline. To provide additional data points for evaluating the segmental tilt angles of the two halves of the peptide, we substituted selected leucines with L-Ala-d_4. Using this approach, we were able to deduce that the apparent average tilt of the C-terminal increases from ∼4° to ∼12° when Pro[10] is introduced. The segment N-terminal to proline is more complex and possibly is more dynamically flexible; Leu to Ala mutations within the N-terminal segment alter the average orientations of alanines in both segments. Nevertheless, in DOPC, we could estimate an apparent kink angle of ∼19°. Together, the results suggest that the central proline influences not only the geometry but also the dynamics of the membrane-spanning peptide. The results make up an important basis for understanding the functional role of proline in several families of membrane proteins.

Transmembrane proteins are integral components of lipid bilayer membranes and exhibit a variety of functions in biological systems. Proline residues often are conserved within the membrane-spanning portions of integral membrane proteins. For example, prolines are conserved in the M_1 segments of GABA receptors (*1*) and acetylcholine receptors (*2*), and in several transmembrane helices of the *Escherichia coli* lactose permease (*3*). Integral nontransport proteins also may contain proline, such as in the IKe phage protein (*4*) and the avian sarcoma virus glycoprotein (*5*). In many of these proteins, the presence of a membrane-embedded proline is likely to be important for function (*6*−*13*). Also in membrane-active peptides such as melittin (*14*, *15*), prolines are sometimes important for function. In spite of their prevalence, the fundamental molecular interactions between membrane lipids and membrane proteins are poorly understood. For this reason, model systems consisting of designed membrane-spanning peptides are helpful for understanding the complex properties of biological membranes. The WALP family of peptides is one such model system that has proven to be useful for elucidating important aspects of the nature of protein−lipid interactions (*16*). WALP peptides are transmembrane peptides consisting of the sequence acetyl-GWW(LA)$_n$LWWA-[ethanol]-amide, in which a variable-length core sequence of alternating Leu/Ala residues generally assumes an α-helical configuration (*17*).

The tryptophan residues at either end of a WALP peptide interact with the bilayer−water interface, producing an anchoring and stabilizing effect, albeit weak, on the peptide helix within a lipid bilayer membrane. Modest anchoring of the peptide probably is accomplished through hydrogen bonding and orientation preferences of the aromatic indole rings (*18*, *19*) with the lipid phosphocholine headgroups and/or water (*20*). Peptide motion is still allowed, and more motional freedom is provided for the Trp side chains at the C-terminus because of the necessity for reorientation of the C-terminal indole rings to interact properly with the lipid bilayer (*20*). Hydrophobic mismatch, namely, the difference between the lengths of the hydrophobic regions of membrane lipids and membrane peptides, has been observed in many studies to have consequences for the orientations and dynamics of both the lipid and peptide components. Nevertheless, WALP peptides in general produce a weaker than expected response to hydrophobic mismatch (*21*, *22*). Potential explanations for the weak response could involve the weak anchoring and the presence of four, possibly competing, tryptophans at different radial and longitudinal positions (*23*−*25*).

WALP19[1] is a 19-residue member of the WALP peptide family (where $n = 6$; above sequence). Having no helix-breaking residues, WALP19 remains a regular helix (unkinked) within lipid bilayers

†This work was supported in part by National Science Foundation Grant MCB 0841227, by the Arkansas Biosciences Institute, and by undergraduate research fellowships to R.T. from the Barry Goldwater Foundation and the Arkansas Department of Higher Education.

*To whom correspondence should be addressed. Telephone: (479) 575-4976. Fax: (479) 575-4049. E-mail: rk2@uark.edu.

[1]Abbreviations: CD, circular dichroism; DLPC, 1,2-dilauroylphosphatidylcholine; DMPC, 1,2-dimyristoylphosphatidylcholine; DOPC, 1,2-dioleoylphosphatidylcholine; Fmoc, fluorenylmethoxycarbonyl; GALA, geometric analysis of labeled alanines; NMR, nuclear magnetic resonance; TEA, triethylamine; TM, transmembrane; WALP19, acetyl-GWWLALALALALALALWWA-ethanolamide.

© 2009 American Chemical Society
Published on Web 11/05/2009

Table 1: Sequences and Deuterium Labeling of Peptides[a]

peptide	sequence
WALP19	a-GWWLALALALALALWWA-e
WALP19-P10	a-GWWLA$^{\#}$LA*LAPALALALWWA-e
WALP19-P10	a-GWWLALALA$^{\#}$PA*LALALWWA-e
WALP19-P10	a-GWWLALALAPALA*LA$^{\#}$LWWA-e
WALP19-P10/A6	a-GWWLA$^{\#}$A*ALAPALALALWWA-e
WALP19-P10/A6	a-GWWLAAALAPALA*LA$^{\#}$LWWA-e
WALP19-P10/A8	a-GWWLA$^{\#}$LAA*APALALALWWA-e
WALP19-P10/A12	a-GWWLALALAPAA*ALA$^{\#}$LWWA-e
WALP19-P10/A12	a-GWWLA$^{\#}$LA*LAPAAALALWWA-e

[a]A* residues were 100% deuterated (Ala-d_4); A$^{\#}$ residues were 60% deuterated. The abbreviation a denotes acetyl; the abbreviation e denotes ethanolamide.

formed by several membrane lipids, including phosphatidylcholines with 12-, 14-, or 18-carbon fatty acyl chains, in which WALP19 exhibits only a small apparent tilt (~4°) from the bilayer normal (*17*). The introduction of a central proline in WALP23 (where $n = 8$ in the above sequence) results in a global "loosening" of the entire WALP helix, not just in the vicinity of the proline itself (*26*). Comparisons among 50 proline-containing transmembrane segments from known membrane protein X-ray crystal structures reveal a wide variety of helix kink angles (*27*), suggesting dynamic flexibility. Furthermore, the helical turn immediately N-terminal to a proline shows a definite tendency toward partial unwinding (*28*).

Despite the highly conserved nature of proline and its potential for a variety of biological roles, the function of proline remains incompletely understood. Due in part to its rigid ring structure, and to the removal of a hydrogen bond (to the $i - 4$ residue), proline will tend to interrupt the backbone structure within a standard α-helix, creating a "kink". The five-membered ring is formed from the aliphatic side chain being joined to both the α-carbon and the amino group, thereby restricting the backbone torsion angle Φ. In spite of the rigid ring, an increased flexibility imparted by proline conceivably could enhance the response to hydrophobic mismatch.

Defined model systems remain valuable resources for addressing specific questions and evaluating predictions concerning protein−lipid interactions. In particular, a system such as WALP19, within an oriented lipid bilayer, provides a direct method for examining proline's contribution to a membrane-spanning segment, in the absence of potential complications due to protein−protein interactions. Additionally, solid-state NMR spectroscopy allows insights into the dynamics as well as the geometry of proline-containing peptides.

For the reasons given above, we have synthesized WALP19 containing proline as the central (tenth) residue, acetyl-G**WW**LALALA**P**ALALAL**WW**A-ethanolamide. Different versions of WALP19-P10 were synthesized, each containing two deuterium-labeled alanine residues (Table 1). In some cases, Leu → Ala-d_4 "mutations" were introduced to provide more deuterated alanine data points for the analysis (Table 1). The designed peptides were then introduced into hydrated, oriented lipid bilayer membranes of DOPC, DMPC, or DLPC and analyzed through solid-state deuterium NMR spectroscopy to examine the influence of the proline within the helix.

MATERIALS AND METHODS

Preparation of Fmoc-L-Ala-d_4. Deuterated L-Ala from Cambridge Isotope Laboratories (Andover, MA) was first derivatized with an N-terminal fluorenylmethoxycarbonyl (Fmoc) protecting group using a previously described protocol with several modifications (*29*). Five millimoles (445 mg) of L-Ala-d_4 was dissolved, with stirring, in 5 mL of water with 5 mmol (700 μL) of triethylamine (TEA) (Mallinckrodt, Paris, KY) in a 250 mL round-bottomed flask. A stir bar was added, and the solution was mixed over a stir plate. A solution of 4.8 mmol (1.62 g) of *N*-(9-fluorenylmethyloxycarbonyloxy)succinimide (Novabiochem, San Diego, CA) in 5 mL of acetonitrile was prepared by gentle heating and was added to the L-Ala-d_4 solution. The reaction mixture was stirred for 4 h at 22 °C; additional TEA was added as necessary to keep the pH between 8.5 and 9.0. The mixture was filtered and the precipitate discarded. The sample was then concentrated by rotary evaporation until the Fmoc-L-Ala-d_4 dried to a thick yellowish gel.

Sixty milliliters of HCl (1.5 N) was added to the concentrated filtrate in 10 mL aliquots, with swirling. The flask was then sonicated for 5−7 min to further disperse and wash the pellet. The suspension was filtered, and the filtrate was discarded. The residue was rinsed with cold methyl *tert*-butyl ether and dried overnight under vacuum (10^{-3} Torr). Crude Fmoc-Ala-d_4 was redissolved in ethyl acetate (10−15 mL) and recrystallized by addition of hexane (~4 mL) followed by cooling and storage at −20 °C for ~48 h.

Solid-Phase Peptide Synthesis. The WALP19-P10 peptides (Table 1) were synthesized using Fmoc-Ala-Wang resin and by "FastMoc" solid-phase synthesis on a Perkin-Elmer (Foster City, CA) Applied Biosystems 433A synthesizer. The resin and nondeuterated Fmoc-protected L-amino acids were from Novabiochem (San Diego, CA) or Advanced Chemtech (Louisville, KY). For deuterium labeling (Table 1), a chosen alanine was incorporated from 100% Fmoc-L-Ala-d_4, along with a second alanine elsewhere in the sequence from 60% Fmoc-L-Ala-d_4 (with 40% nondeuterated Fmoc-L-Ala).

Peptides were finished by coupling acetyl-Gly in the final N-terminal position and were cleaved from the resin (48 h, 22 °C) using 20% ethanolamine in dichloromethane (*30*). Following filtration to remove the resin, the solvent volume was reduced by rotary evaporation. Peptides were precipitated from minimal volumes of ethanolamine and dichloromethane by addition of excess deionized water, left overnight at 4 °C, and centrifuged for 2 h at 24000*g*. The recovered pellet was dried overnight in vacuo (10^{-3} Torr). Peptide purity was assessed by reversed-phase HPLC using a 4.6 mm × 50 mm Zorbax SB-C8 column packed with 3.5 μm octyl-silica (Agilent Technologies, Santa Clara, CA), operated at 1 mL/min using a methanol/water gradient from 85 to 99% methanol over 5 min. HPLC solvents contained 0.1% trifluoroacetic acid. Chromatograms showed only one major peptide peak (Figure S1 of the Supporting Information). Molecular masses of peptides, and extents of deuteration, were verified using matrix-assisted laser desorption ionization mass spectrometry (Figure S2 of the Supporting Information). Peptides were quantitated on the basis of UV absorbance at 280 nm, using an ε of 5600 Trp^{-1} M^{-1} cm^{-1} (*31*).

Oriented Sample Preparation. Synthetic deuterated peptides were incorporated into hydrated lipid bilayers of DOPC, DMPC, or DLPC (from Avanti Polar Lipids, Alabaster, AL). A peptide/lipid mixture (1/40 in 95% methanol and 5% water) was evenly applied on 40 glass slides (4.8 mm × 23 mm × 0.07 mm) (Marienfeld, Lauda-Konigshofen, Germany) and dried under vacuum (10^{-3} Torr) for 48 h. The slides were then hydrated 45% (w/w) with ^{2}H-depleted water from Cambridge, stacked,

and sealed in a cuvette. The samples were allowed to orient into a liquid crystalline phase during incubation at 40 °C for at least 48 h.

Solid-State NMR Spectroscopy. NMR measurements were taken using a Bruker (Billerica, MA) Avance-300 spectrometer. The alignment of the lipid bilayers in each glass plate sample was confirmed by ^{31}P NMR (*17*) (see Figure S3 of the Supporting Information). The ^{2}H experiments were performed for $\beta = 0°$ and $\beta = 90°$ sample orientations, using a quadrupolar echo pulse sequence (*32*) with full phase cycling, a 90° pulse time of 3.2 μs, an echo delay of 110 μs, an interpulse time of 90 ms, and 0.6−0.8 million scans. A 100 Hz line broadening was applied to the ^{2}H spectra. Measurements were taken at 50 °C when the lipids were in the liquid crystalline phase, and spectral resolution and signal intensities are good (*20*).

Circular Dichroism Spectroscopy. DLPC small unilamellar vesicle samples having a peptide/lipid ratio of 1/40 were prepared by sonication as described in ref *33*. Circular dichroism (CD) spectra were recorded at 22−24 °C using a Jasco (Easton, MD) J710 CD spectropolarimeter with a 1 mm path length cell, a 1.0 nm bandwidth, a 0.2 nm step resolution, and a 20 nm/min scan speed. Each spectrum is an average of 10 scans.

GALA Analysis. The ^{2}H NMR data for the oriented peptides were analyzed using the GALA (geometric analysis of labeled alanines) method described by van der Wel (*17*), implemented in Microsoft Excel. The quadrupolar splittings ($\Delta\nu_q$) from the alanine CD_3 groups follow eq 1.

$$\Delta\nu_q = \frac{3}{2} S_{zz} \frac{e^2qQ}{h} \left[\frac{1}{2}(3\cos^2\theta - 1)\right]\left[\frac{1}{2}(3\cos^2\beta - 1)\right]\left[\frac{1}{2}(3\cos^2\gamma - 1)\right] \quad (1)$$

where the term $(e^2qQ)/h$ is the quadrupolar coupling constant, which has a static value of ~168 kHz for aliphatic deuterons (*34*). The term S_{zz} is a principal order parameter for estimating molecular motion. The GALA fits for WALP peptides are relatively insensitive to S_{zz} in the range of 0.7−0.9 (*17*, *20*, *35*). The quadrupolar splitting $\Delta\nu_q$ depends upon three angles: the known angle β (either 0° or 90° depending upon macroscopic sample orientation) between the membrane normal and the magnetic field, the known angle γ (109.5°, the "tetrahedral" angle) between a C_β−^{2}H bond and the C_α−C_β axis of methyl rotation for the Ala side chain, and the key variable θ, the angle between a particular C_α−C_β bond and the membrane normal (*17*). As described by van der Wel (*17*), θ depends upon the peptide rotation angle ρ (relative to the reference C_α of Gly^{1}, defining the direction of the tilt), the magnitude of the peptide tilt angle τ, and importantly the detailed alanine geometry described by $\varepsilon_\parallel$, an angle between the alanine C_α−C_β bond and the peptide's helix axis. (Each alanine in an undistorted α-helix, or helical segment, will exhibit the same constant value of $\varepsilon_\parallel$.) Using these relationships, τ, ρ, and $\varepsilon_\parallel$ values were varied for the helix (or segment) to give the best agreement between calculated and observed $\Delta\nu_q$ values (*17*). The fits varied little for choices of S_{zz} between 0.8 and 0.9 (see also Figure S4 of the Supporting Information). A two-dimensional (τ, ρ) matrix for a user-defined $\varepsilon_\parallel$ value was created in Excel, and an interactive grid search was used to determine parameters that gave the lowest root-mean-square deviation (rmsd) values.

RESULTS

Circular dichroism spectra (Figure 1) show that the α-helical nature of lipid membrane-incorporated WALP19 is modestly

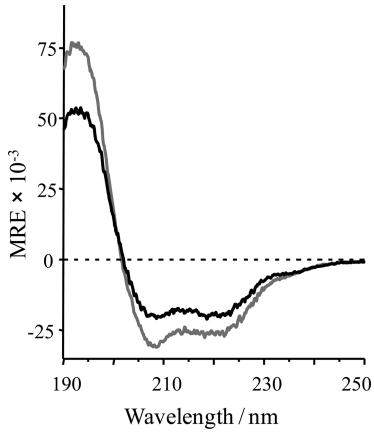

FIGURE 1: CD spectra for WALP19 (gray) and WALP19-P10 (black), dispersed in DLPC vesicles at a 1/40 peptide/lipid ratio, at 22 °C.

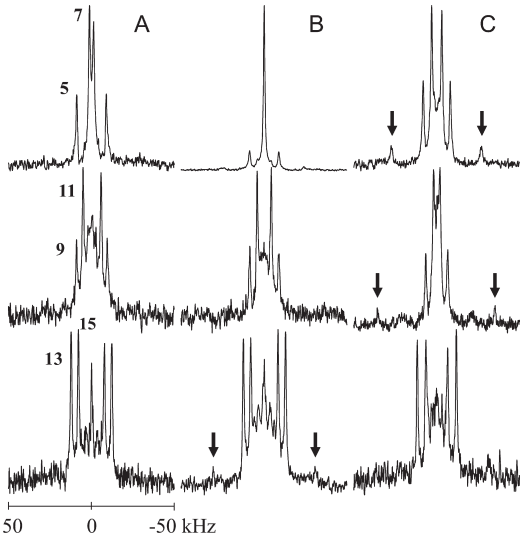

FIGURE 2: ^{2}H NMR spectra, with assignments, for labeled alanines in WALP19-P10. Peptides were oriented at β = 0° in hydrated bilayers of (A) DLPC, (B) DMPC, and (C) DOPC. The peak assignments for Ala methyls in the peptide sequence are shown for the DLPC spectra. Selected peaks from C_α deuterons are marked with arrows. The temperature was 50 °C.

decreased but not abolished by Pro^{10}. The characteristic ratio $\varepsilon_{222}/\varepsilon_{208}$ (*36*) changes from ~0.96 to ~1.00 when Pro^{10} is introduced into WALP19, and the positive ellipticity at 195 nm is diminished by ~30%. The spectral comparison (Figure 1) illustrates these effects, as well as the overall less negative ellipticity between 200 and 235 nm when Pro^{10} is present.

Further information about the proline effect was obtained from deuterium (^{2}H) NMR spectra. In Figure 2 are shown the spectra for the six labeled core alanines of WALP19-P10 incorporated into oriented, hydrated bilayer membrane samples using three different lipids. Present in each spectrum are two prominent pairs of peaks representing the methyl CD_3 groups from two labeled alanines in the WALP19-P10 sequence. In most cases, the major pairs of peaks can be assigned to the respective alanines, labeled at 60 and 100%, based upon the relative peak intensities. [For alanines 13 and 15, assignments were made when only A^{15} was labeled in a related peptide having A^{12} instead of L^{12} (see below).] When samples were turned from $\beta = 0°$ (Figure 2) to β = 90° (not shown), all peaks were still observed as sharp

Table 2: Observed $\Delta\nu_q$ Values[a] for Core Alanine Methyl Groups in WALP19 and WALP19-P10 in Three Lipids

	DLPC		DMPC		DOPC	
Ala	L^{10}[b]	P^{10}	L^{10}[b]	P^{10}	L^{10}[b]	P^{10}
5	7.2	17.3	6.6	17.2	4.4	16.1
7	3.3	3.6	7.8	0.0	11.4	6.0
9	11.3	18.6	8.7	17.5	7.0	13.1
11	2.6	10.8	4.6	8.6	6.8	3.9
13	14.0	24.2	12.8	25.0	11.9	23.1
15	0.0	15.6	0.0	16.3	1.5	12.9

[a]Values in kilohertz. [b]Data for native WALP19-L10 from ref *17*.

resonances and the quadrupolar splittings were reduced by a factor of 2. This comparison of spectra for $\beta = 0°$ and $\beta = 90°$ sample orientations indicates rapid rotational diffusion, namely that the reorientation of WALP19-P10 about the lipid bilayer normal is rapid with respect to the NMR time scale (*17*, *37*). Phosphorus (^{31}P) NMR spectra, which monitor the lipid headgroups (Figure S3 of the Supporting Information), confirm that the lipids are configured primarily as well-oriented bilayers in these aligned, hydrated samples, although small amounts of unaligned material also are present.

In addition to the major pairs of peaks representing two labeled alanine methyl groups, also evident in Figure 2 are additional paired resonances that are weaker and broader and represent (generally) larger quadrupolar splittings. Similar resonances have been assigned to backbone C_α deuterons in gramicidin channels (*37*, *38*), although they could not be resolved with certainty for any backbone deuterons in WALP19 (*17*). In the NMR spectra from aligned deuterated peptides, it is typical that the methyl rotation leads to not only a 3-fold reduction in $\Delta\nu_q$ but also apparently a line narrowing along with a $\gg$3-fold increase in peak height (Figure 2). Nevertheless, a comparison of Figure 2 with the corresponding ^2H NMR spectra for WALP19 core alanines (*17*) suggests that several of the backbone C_α deuterons apparently are "unmasked" by the presence of Pro^{10}. (Other backbone deuterons could exhibit lower quadrupolar splittings that would be obscured by the strong methyl signals.) We attribute the newly observed WALP backbone C_α−D resonances to an altered peptide dynamics when proline is present within the core sequence (see Discussion).

The assignments for the WALP19-P10 core alanine methyl ^2H quadrupolar splittings are listed in Table 2, along with the corresponding values for WALP19 itself (*17*). It is evident that the presence of Pro^{10} instead of Leu^{10} causes large changes in many of the alanine side-chain methyl $\Delta\nu_q$ values. [The observed backbone C_α−D resonances were not assigned because (a) two signals were not necessarily observed in every spectrum and (b) the weak intensities did not necessarily scale with the percent deuteration of two different alanines. "Extra" peaks having zero or low $\Delta\nu_q$ values also were not assigned; we attribute such peaks to a combination of minor peptide impurities, unaligned material giving "breakthrough" peaks for a nominal $\beta = 90°$ orientation, and residual HDO in the solvent.]

The six available assigned methyl $\Delta\nu_q$ values for core alanine side chains were fit using the GALA method (*17*), with results shown in Figure 3. Regardless of the bilayer lipid identity, DOPC, DMPC, or DLPC, it is evident that the set of six data points does not fit a tilted regular helix. Rather, even for the best fit in each lipid bilayer (Figure 3), several of the $\Delta\nu_q$ data points

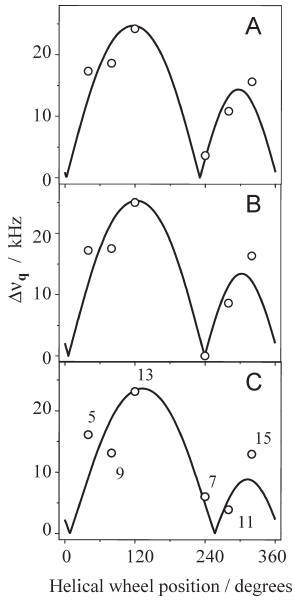

FIGURE 3: GALA helical waves based upon six assigned core alanine methyl ^2H quadrupolar splittings for WALP19-P10 in three lipids, from the spectra in Figure 2: (A) DLPC, (B) DMPC, and (C) DOPC. The alanines are numbered in panel C and have the same helical wheel positions in panels A and B. The rmsd values are high for all curves, suggesting helix distortion.

are far off the curve that describes a uniform tilted helix. The likely explanation is that Pro^{10} has distorted the helix, such that the six data points cannot be fit as a single unit. For this reason, we sought to analyze individually the tilt of segments N-terminal and C-terminal to the proline. For this purpose, it would be advantageous to have more than three data points for each peptide segment.

To introduce more deuterated alanines for the segmental analysis, several selected leucines (L^6, L^8, and L^{12}) were replaced, one at a time, with L-Ala-d_4. As controls for each new "mutated" peptide, a second L-Ala-d_4 was included on the same side of the proline; thus, A^5 was deuterated along with either A^6 or A^8, or A^{15} with A^{12} (Table 1). The strategy (adapted from ref *24*) allowed monitoring of a control Ala methyl $\Delta\nu_q$ value before and after each selected Leu → Ala substitution.

Results with the Leu → Ala substituted peptides in the three lipids are shown in Figure 4. From each spectrum can be measured $\Delta\nu_q$ for the new L-Ala-d_4 together with $\Delta\nu_q$ for the control (previously labeled) L-Ala-d_4. The results reveal that, in response to $L^{12} \rightarrow A^{12}$ substitution, the quadrupolar splitting for Ala^{15} changes little in DMPC or DOPC yet decreases ~4 kHz in DLPC (Table 3). The changes in $\Delta\nu_q$ for A^5 are larger in all lipids, in response to L → A replacements at position 6 or 8; in several cases, $\Delta\Delta\nu_q$ goes as high as 5 kHz (Table 3). With these results in hand, we sought to obtain additional information by labeling additional alanines in the L^6A and $L^{12}A$ variants of WALP19-P10. We therefore labeled A^{13} and A^{15} in WALP19-P10/A6, as well as A^5 and A^7 in WALP19-P10/A12 (Table 1). The ^2H NMR spectra for the labeled alanines in these "mutants" of WALP19-P10 (Figure S5 of the Supporting Information) revealed, once again, larger changes in ^2H $\Delta\nu_q$ values in response to the L^6A mutation, preceding the proline, than to the $L^{12}A$ mutation, following the proline. Importantly, the effects of each mutation, whether large or small, are similar on both sides of the proline (Table 3). We summarize these results in Figure 5 and deduce that the detailed peptide properties, geometry and orientation,

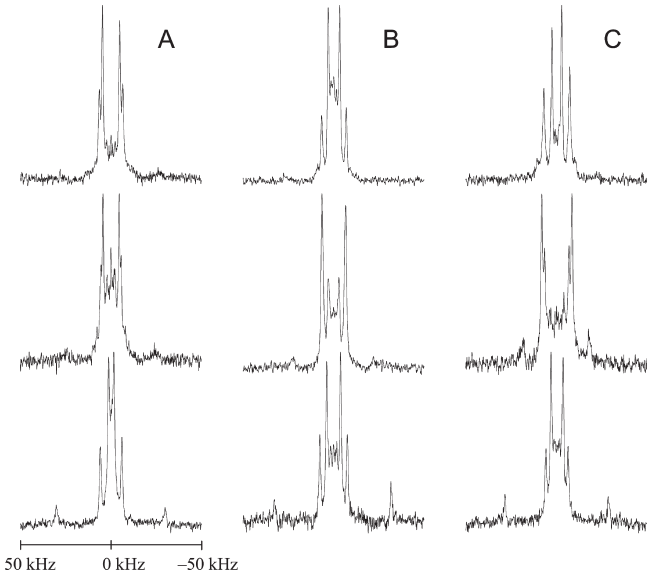

FIGURE 4: Deuterium NMR spectra (β = 0°) of L6A, L8A, and L12A (top to bottom) variants of WALP19-P10 in (A) DLPC, (B) DMPC, and (C) DOPC. In each peptide, the new alanine is 100% deuterated, giving the taller peaks. A second control alanine is 60% deuterated, either A^5 (top and middle) or A^{15} (bottom). Several backbone C_α deuteron signals also are evident. The temperature is 50 °C.

Table 3: Observed $\Delta\nu_q$ Values[a] for Selected Alanine Methyl Groups in WALP19-P10 and Several Leu/Ala Mutants in Three Lipids

Ala	mutant	DLPC	DMPC	DOPC
5	none[b]	17.3	17.2	16.1
	$L^{12}A$	15.9	16.6	16.9
	$L^{8}A$	11.0	12.8	13.4
	$L^{6}A$	12.2	13.4	14.1
15	none[b]	15.6	16.3	12.9
	$L^{12}A$	11.6	15.1	12.0
	$L^{6}A$	8.4	13.0	11.2
7	none[b]	3.6	0.0	6.0
	$L^{12}A$	1.6	0.9	7.2
13	none[b]	24.2	25.0	23.1
	$L^{6}A$	19.4	23.1	22.3

[a]Values in kilohertz. [b]Native WALP19-P10 sequence.

are more sensitive to the detailed sequence preceding the proline than to the sequence following the proline. It is further evident that the effects of the Leu to Ala substitutions is much larger in DLPC than in DOPC (Figure 5 and Table 3). On the basis of these findings, it is feasible to define an apparent average magnitude and direction of tilt for the C-terminal segment of WALP19-P10 in each of the three lipids, but for the N-terminal segment only in DOPC, where the influence of Leu → Ala mutations is less pronounced (Figure 5).

The best available GALA fits for the segment C-terminal to Pro^{10} in three lipids are based upon quadrupolar splittings from four Ala methyl groups (Figure 6). The data points for Ala^{15} are closely similar for Ala^{12} versus Leu^{12} in DMPC and DOPC, while the difference is larger in DLPC. In all cases, an average $\Delta\nu_q$ (between the values observed with Ala^{12} and Leu^{12}) was used to fit Ala^{15} (Figure 5). With a caveat for DLPC, due to the 4 kHz change in $\Delta\nu_q$ for A^{15}, the GALA fits appear to be excellent in all three lipids, giving appropriate values for rmsd and $\varepsilon_{||}$ for the Ala side-chain geometry (*17*), and a similar apparent static tilt of

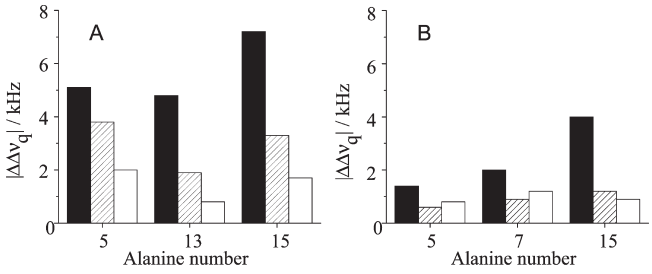

FIGURE 5: Changes in ^2H quadrupolar splittings for selected Ala methyl groups due to Leu → Ala mutations in WALP19-P10 variants incorporated into DLPC (black), DMPC (hatched), or DOPC (white) hydrated bilayers: (A) L^6A sequence variant and (B) $L^{12}A$ sequence variant. Absolute values of $\Delta\Delta\nu_q$ and alanine positions are indicated.

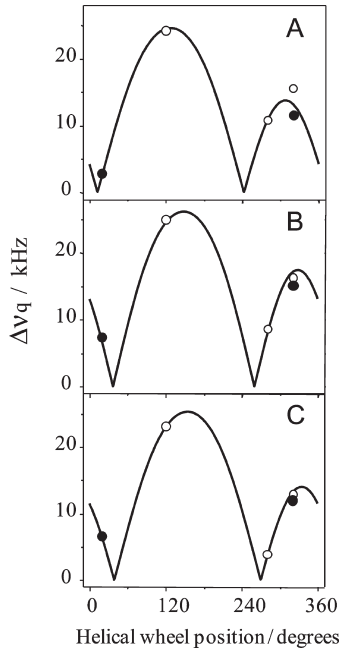

FIGURE 6: GALA helical waves for the C-terminal segment of WALP19-P10 in three lipids: (A) DLPC, (B) DMPC, and (C) DOPC. Signals from the $L^{12}A$ variant are shown as filled circles (with A^{12} at 20° and A^{15} at 320° helical wheel positions). S_{zz} was set to 0.87 (see also Figure S4 of the Supporting Information).

Table 4: Apparent Tilt Magnitude and Direction for the C-Terminal Segment of WALP19-P10, Compared to WALP19 Itself (L10), in Three Lipids[a]

	DLPC		DMPC		DOPC	
	L^{10b}	P^{10}	L^{10b}	P^{10}	L^{10b}	P^{10}
τ (deg)	4.0	11.6	3.6	13.2	4.0	11.9
ρ (deg)	171	171	195	192	218	198
$\varepsilon_{||}$ (deg)	58.8	59.0	59.0	58.7	59.2	59.2
rmsd (kHz)	0.5	0.3	0.5	1.0	0.5	0.5

[a]Best-fit GALA values; method from ref *17*, using an S_{zz} value of 0.87. See also Figure 5. [b]Fits for WALP19-L10 from ref *17*.

~12−13° in the three different lipid bilayer membranes (Table 4). To confirm that the favorable results were not due to overfitting the data, we fixed the $\varepsilon_{||}$ value at 58.0°, leaving only τ and ρ as free parameters. The analysis with a fixed $\varepsilon_{||}$ led to similar τ and ρ values, while the rmsd did not exceed 1.2 kHz, attesting to the

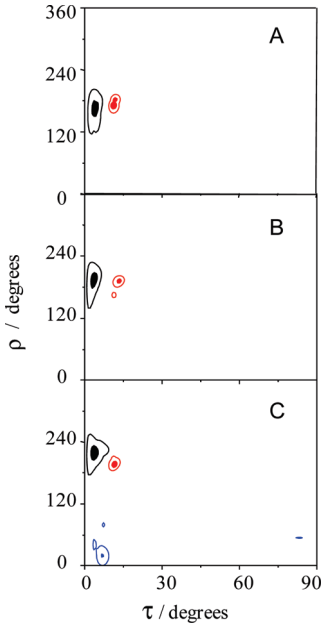

FIGURE 7: rmsd contour plots for WALP19 (black) and the C-terminus of WALP19-P10 (red) in (A) DLPC, (B) DMPC, and (C) DOPC. S_{zz} was set to 0.87 (see also Figure S4 of the Supporting Information). The *x*-axis angle τ is the magnitude of segment tilt; the *y*-axis angle ρ is the prior rotation of the segment relative to C_α of Gly[1], effectively defining the direction of tilt (see also ref *17*). The contour levels for rmsd are 1.5 (solid fill) and 3.0 kHz. Contour levels (blue) are also shown for the N-terminus of WALP19-P10 in DOPC, using data points from A^5, A^6, A^7, and A^8. The estimated apparent kink angle in DOPC is ~19°. See also Figure 8.

validity of the results, as summarized in Table 4. From GALA fits, the peptide rotation or direction of tilt (ρ angle) is uncertain to ~10−15° (*17*). Within experimental error and the uncertainty of the fitting, the range of accessible ρ direction of tilt values for the C-terminal does not change in any of the three lipids, with or without Pro^{10} (Table 4). The apparent static tilt of the C-terminal segment estimated by GALA increases almost 10° in each lipid.

It also is useful to compare the (τ, ρ) contour plots for WALP19 and WALP19-P10 in the three lipids (Figure 7). These plots illustrate directly the increase in τ and the similar ρ distributions in each lipid, with and without Pro^{10}. For the DOPC environment, we also tested the influence of different assumed values of S_{zz} from 0.6 to 0.9 upon the apparent tilt of the C-terminal segment (Figure S4 of the Supporting Information). When S_{zz} is lowered from 0.8 to 0.6, the apparent τ increases from 12.8° to 18° (Figure S4), but rmsd and $\varepsilon_{||}$ also increase, indicating a poorer quality of the fit. The apparent ρ is in all cases unaffected by the choice of S_{zz}.

With regard to the segment N-terminal to Pro^{10}, several issues remain. In particular, residue 9 fits poorly in all data sets (Figure 3). Furthermore, global peptide properties are sensitive to the identity of residues 6 and 8 (Figures 4 and 5, Figure S5 of the Supporting Information, and Table 3), making it difficult to acquire sufficient data points for a consistent set of labeled alanines to define the apparent N-terminal tilt. For these reasons, the assignment of an apparent tilt angle remains problematic for the segment N-terminal to Pro^{10} in DLPC or DMPC. Nevertheless, a reasonable estimate is available for WALP19-P10 in DOPC (Figure 7C).

If the data from all Ala residues (including Leu to Ala substitutions) from the segment N-terminal to Pro^{10} are considered (residues 5−9, in DOPC), the GALA fit yields a poor

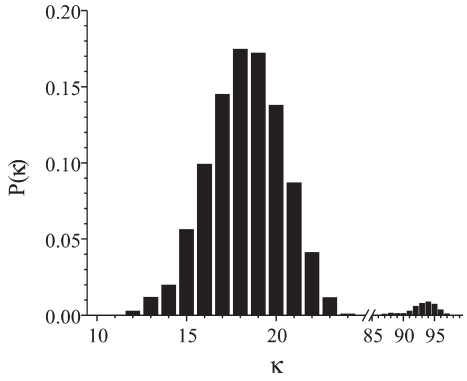

FIGURE 8: Distribution of apparent kink angles, κ (degrees), calculated from rmsd (τ, ρ) analysis of N- and C-terminal segments of WALP19-P10 in DOPC (Figure 7C). Regions with a rmsd of < 3 kHz were binned at a τ of 0.5° and a ρ of 3°, resulting in 122 points for the N-terminus and 76 points for the C-terminus.

rmsd of 2.4 kHz. Visual inspection reveals that the major cause is a deviation of Ala^9 from the rest of the curve. This result is expected, since the Pro-induced distortion nearly always involves at least one preceding residue (*27*, *28*, *39*). If the Ala^9 data point is excluded from the analysis, the rmsd is reduced to 1.4 kHz, with the fit to (τ, ρ, $\varepsilon_{||}$) being (7.0°, 20°, 59.0°). (A second minimum with a rmsd of 1.0 kHz is also observed, but the $\varepsilon_{||}$ value of 56.5° is too low.) To confirm that the reduction of rmsd is not just due to a decreased sampling of data, we tested exclusion of other individual data points from Ala residues 5−8. Each test (with the Ala^9 data point present) led either to a rmsd of > 1.8 kHz or to an unrealistic $\varepsilon_{||}$ value (< 57° or > 60°). Furthermore, the (τ, ρ) values were similar in all cases where an individual Ala residue was discarded. Apparent average (τ, ρ) values of (7°, 20°) are therefore reasonable for the N-terminal segment of WALP19-P10.

With the orientations of N- and C-terminal parts of the peptide in hand, although only for DOPC, it is possible to estimate an apparent kink angle in the DOPC environment, induced by Pro^{10}. Using eq 2, derived previously (*24*)

$$\kappa = a\cos[\sin(\tau_N) \times \sin(\tau_C) \times \cos(\Delta\rho) + \cos(\tau_N) \times \cos(\tau_C)] \quad (2)$$

the calculated kink angle (κ) is ~19°. The uncertainty in the kink can be represented by a distribution of apparent kink angles (Figure 8) based upon the ranges of accessible orientations (Figure 7C) for the N- and C-terminal segments of WALP19-P10 in DOPC. The variability observed for the control alanine signals in the mutant peptides also is compatible with this distribution.

DISCUSSION

It is widely recognized that an internal proline should disrupt or even "break" an α-helix. An early survey of 291 helices in 57 crystal structures of water-soluble proteins (*40*) included 10 helices containing an internal proline. These prolines were observed in relatively long helices (having four to eight helical turns) and induced an average kink angle of ~26°. The backbone hydrogen bond between NH_{i+1} and O_{i-3} (where *i* is the sequence number for Pro) also was observed to break (*40*). A further study involving 48 proline-containing helices in soluble protein structures (*41*) revealed an average kink angle of 25°, with a range from 9° to 41°. It was further noted that proline induced a relative

rotation of ±50° between the helical segments on either side of Pro (*41*).

Regardless of its potential for helix disruption, proline commonly is found in the middle of (putative) TM helical segments (*42*). Indeed, wide ranges of Pro-induced kink angles and relative segmental rotations have been observed directly in TM helices. Kink angles between 0° and 70°, together with a full range (±180°) of relative rotation (or "swivel") angles, were observed for 50 Pro-containing TM helices in crystal structures of 20 membrane proteins (*27*), with 50% of the kink angles falling between 10° and 25°. Additionally, the ϕ and ψ torsion angles showed systematic deviations among the four residues preceding proline in 27 TM helices from membrane protein crystal structures, and a parallel pattern was observed in molecular dynamics simulations of Pro-interrupted poly-Ala helices (*28*).

In this work, we have investigated the influence of proline upon the single, isolated TM helix of WALP19. This experimental system allowed us to investigate a "pure" helix with only lipid neighbors, in the absence of protein−protein interactions. The ^{2}H NMR spectra when $\beta = 90°$ argue for fast axial reorientation and against aggregation of the WALP19 or WALP19-P10 peptides. Earlier pyrene excimer experiments (*43*) further indicated an absence of pairwise helix interactions when the WALP23/DOPC ratio was below 1/25. The shorter WALP19 and derivatives should therefore remain monomeric at 1/40 in DMPC and DLPC as well as DOPC.

The presence of Pro^{10} alters the peptide backbone dynamics. Previously, it was observed that introduction of Pro^{12} into WALP23 causes a 10-fold increase in the rate of backbone H−D exchange over the entire TM segment (*26*), suggesting increased backbone dynamics. In concert with the isotope exchange kinetics for WALP23-P12, we now observe previously "silent" backbone C_α−D resonances for labeled alanines in WALP19-P10, again suggesting increased backbone dynamics. These proline effects seem to concern local dynamics of peptide planes within the larger helical structure. [Interestingly, glycine—also a potential helix "breaker" (*42*), though weaker than proline—does not influence the rate of backbone H−D exchange for WALP23 in lipid bilayers (*26*).]

Considerations of global dynamics will influence the interpretation of NMR spectra and GALA fits. In particular, it is possible that large-scale peptide motions in combination with large tilt angles can fit the observed quadrupolar splitting data (*44*, *45*), leading to a multiplicity of solutions. It is nevertheless expected, from the peptide plane geometry and orientation within a helix, that the ^{15}N−^{1}H dipolar couplings should exhibit different sensitivity than the ^{2}H quadrupolar splittings to molecular motion (*44*, *45*). Furthermore, it has been noted that the ^{15}N−^{1}H dipolar couplings ["PISEMA" method (*46*, *47*)] generally will yield the correct mean values of TM peptide tilt and azimuthal rotation angle using static models (*48*). It is therefore significant that, for the cases tested to date (*25*, *49*), the GALA and PISEMA approaches using essentially static models (incorporating only a principal order parameter) have converged to the same values for the average direction and magnitude of TM peptide tilt. Regardless of the motion, it is clear that a single helix will not fit the quadrupolar splittings for the core alanines of WALP19-P10 (Figure 3). Using four Ala data points and a static model with order parameter, we could discern an approximate 10° change in the tilt of the C-terminal segment when Pro^{10} is introduced (Figure 5). The small number of data points precluded testing of more complex motional models.

With regard to the N-terminus, the Ala^9 methyl ^{2}H quadrupolar splitting appears not to fit a helical model. Furthermore, Leu to Ala substitutions N-terminal to Pro^{10} affect peptide properties globally (as monitored by the alanine sidechain ^{2}H quadrupolar splittings), suggesting that the helical structure is less well-defined in the N-terminal region. The findings agree with the variation in ϕ and ψ torsion angles observed N-terminal to proline in protein crystal structures (*27*) and when Pro is introduced into poly-Ala helices (*28*). It is noteworthy that we can better define the geometry and tilt of the helical segment that is C-terminal to proline. With Ala^9 (preceding proline) effectively unavailable for the GALA tilt analysis, it is clear that more samples having more available alanine data points, and without mutations, will be needed to clarify the limitations on the N-terminal tilt analysis.

As noted, within a survey of 50 TM helices in protein crystal structures, Cordes et al. (*27*) found a wide distribution of kink angles. When two turns of helix C-terminal to Pro were superimposed, the N-terminal segments displayed tilt angles from 0° to >60° together with a full range of "swivel" angles (±180°) for rotation of one segment relative to the other. Larger tilt angles were associated with the swivel hemisphere defined by a $\Delta\rho$ of $180 \pm 90°$. The overall picture suggests a variable kink angle and a somewhat flexible N-terminus, particularly in light of the variations in (ϕ, ψ) angles within the 1.5 helical turns immediately preceding proline (*27*, *28*). Our composite results for WALP19-P10 are consistent with this view.

For the particular case of WALP19-P10 in DOPC (Figure 7C), we have a reasonable estimate of a swivel angle ($\Delta\rho$) of ∼180°, based upon a ρ of ∼198° for the C-terminus (Table 4) minus ∼20° for the N-terminus (see Results). Regardless of molecular motions, there is general agreement among solid-state NMR and computational methods concerning predictions of the ρ angle defining the direction of tilt (*25*, *44*, *45*, *48*, *50*). When $\Delta\rho$ is ∼180°, the N- and C-terminal segmental tilts approximately add to give the kink angle (eq 2, above). An estimated average kink angle of ∼19° therefore derives from the C-terminus being tilted ∼12° from the membrane normal and the N-terminus being tilted ∼7° in the opposite direction. Such a kink angle of ∼19° is comparable to that observed in melittin (*15*) and is consistent with "typical" values for proline kinks in helices from both soluble (*40*, *41*) and transmembrane (*27*, *28*) proteins. Nevertheless, because complex motional averaging could reduce the observed quadrupolar splittings and the deduced tilt angles (*44*, *45*), while preserving the apparent ρ angles, the actual segmental tilts could be larger than 7° and 12° for the respective N- and C-termini. Dynamic considerations therefore suggest that the estimated most probable apparent kink angle of 19° in DOPC (Figure 8) should be considered a lower limit. The similar apparent tilts of the N- and C-terminal segments, each with respect to the bilayer membrane normal, not only give rise to the lower limit for the kink angle but also permit each of the Trp indole anchors to remain relatively close to the membrane−water interface.

ACKNOWLEDGMENT

We thank Johanna M. Froyd-Rankenberg and Christopher Mazzanti for helpful discussions and Marvin Leister for invaluable assistance with the NMR spectrometer.

SUPPORTING INFORMATION AVAILABLE

HPLC profiles of WALP19 and WALP19-P10 (Figure S1), mass spectrum of synthetic WALP19-P10 having 1.6 residues of Ala-d_4 (Figure S2), ^{31}P NMR spectra of WALP19-P10 in DLPC, DMPC, and DOPC (Figure S3), fits of the C-terminal segment of WALP19-P10 in DOPC (Figure S4), and deuterium NMR spectra ($\beta = 0°$) of Leu → Ala variants of WALP19-P10 in hydrated lipid bilayer membranes (Figure S5). This material is available free of charge via the Internet at http://pubs.acs.org.

REFERENCES

1. Greenfield, L. J., Zaman, S. H., Sutherland, M. L., Lummis, S. C. R., Niemeyer, M. I., Barnard, E. A., and Macdonald, R. L. (2002) Mutation of the Gaba(a) Receptor M1 Transmembrane Proline Increases Gaba Affinity and Reduces Barbiturate Enhancement. *Neuropharmacology 42*, 502–521.
2. De Planque, M. R. R., Rijkers, D. T. S., Fletcher, J. I., Liskamp, R. M. J., and Separovic, F. (2004) The α-M1 Segment of the Nicotinic Acetylcholine Receptor Exhibits Conformational Flexibility in a Membrane Environment. *Biochim. Biophys. Acta 1665*, 40–47.
3. Abramson, J., Smirnova, I., Kasho, V., Verner, G., Kaback, H. R., and Iwata, S. (2003) Structure and Mechanism of the Lactose Permease of *Escherichia coli*. *Science 301*, 610–615.
4. Williams, K. A., Farrow, N. A., Deber, C. M., and Kay, L. E. (1996) Structure and dynamics of bacteriophage IKe major coat protein in MPG micelles by solution NMR. *Biochemistry 35*, 5145–5157.
5. Delos, S. E., Gilbert, J. M., and White, J. M. (2000) The central proline of an internal viral fusion peptide serves two important roles. *J. Virol. 74*, 1686–1693.
6. Von Heijne, G. (1991) Proline kinks in transmembrane α-helices. *J. Mol. Biol. 218*, 499–503.
7. Sansom, M. S. P., and Weinstein, H. (2000) Hinges, Swivels and Switches: The Role of Prolines in Signalling Via Transmembrane α-Helices. *Trends Pharmacol. Sci. 21*, 445–451.
8. Govaerts, C., Blanpain, C., Deupi, X., Ballet, S., Ballesteros, J. A., Wodak, S. J., Vassart, G., Pardo, L., and Parmentier, M. (2001) The Txp Motif in the Second Transmembrane Helix of Ccr5: A Structural Determinant of Chemokine-Induced Activation. *J. Biol. Chem. 276*, 13217–13225.
9. Stitham, J., Martin, K. A., and Hwa, J. (2002) The Critical Role of Transmembrane Prolines in Human Prostacyclin Receptor Activation. *Mol. Pharmacol. 61*, 1202–1210.
10. Orzaez, M., Salgado, J., Gimenez-Giner, A., Perez-Paya, E., and Mingarro, I. (2004) Influence of Proline Residues in Transmembrane Helix Packing. *J. Mol. Biol. 335*, 631–640.
11. Kinclova-Zimmermannova, O., Zavrel, M., and Sychrova, H. (2005) Identification of Conserved Prolyl Residue Important for Transport Activity and the Substrate Specificity Range of Yeast Plasma Membrane Na^+/H^+ Antiporters. *J. Biol. Chem. 280*, 30638–30647.
12. Joshi, A. D., and Pajor, A. M. (2006) Role of Conserved Prolines in the Structure and Function of the Na^+/Dicarboxylate Cotransporter 1, Nadc1. *Biochemistry 45*, 4231–4239.
13. Peralvarez-Marin, A., Lorenz-Fonfria, V. A., Simon-Vazquez, R., Gomariz, M., Meseguer, I., Querol, E., and Padros, E. (2008) Influence of Proline on the Thermostability of the Active Site and Membrane Arrangement of Transmembrane Proteins. *Biophys. J. 95*, 4384–4395.
14. Smith, R., Separovic, F., Milne, T. J., Whittaker, A., Bennett, F. M., Cornell, B. A., and Makriyannis, A. (1994) Structure and orientation of the pore-forming peptide, melittin, in lipid bilayers. *J. Mol. Biol. 241*, 456–466.
15. Lam, Y. H., Wassall, S. R., Morton, C. J., Smith, R., and Separovic, F. (2001) Solid-State NMR Structure Determination of Melittin in a Lipid Environment. *Biophys. J. 81*, 2752–2761.
16. Killian, J. A., Salemink, I., De Planque, M. R., Lindblom, G., Koeppe, R. E., II, and Greathouse, D. V. (1996) Induction of nonbilayer structures in diacylphosphatidylcholine model membranes by transmembrane α-helical peptides. Importance of hydrophobic mismatch and proposed role of tryptophans. *Biochemistry 35*, 1037–1045.
17. Van der Wel, P. C. A., Strandberg, E., Killian, J. A., and Koeppe, R. E., II (2002) Geometry and intrinsic tilt of a tryptophan-anchored transmembrane α-helix determined by ^{2}H NMR. *Biophys. J. 83*, 1479–1488.
18. Separovic, F., Hayamizu, K., Smith, R., and Cornell, B. A. (1991) Carbon-13 chemical shift tensor of L-tryptophan and its application to polypeptide structure determination. *Chem. Phys. Lett. 181*, 157–162.
19. Separovic, F., Gehrmann, J., Milne, T., Cornell, B. A., Lin, S. Y., and Smith, R. (1994) Sodium ion binding in the gramicidin A channel. Solid-state NMR sutides of the tryptophan residues. *Biophys. J. 67*, 1495–1500.
20. van der Wel, P. C. A., Reed, N. D., Greathouse, D. V., and Koeppe, R. E., II (2007) Orientation and motion of tryptophan interfacial anchors in membrane-spanning peptides. *Biochemistry 46*, 7514–7524.
21. De Planque, M. R. R., Greathouse, D. V., Koeppe, R. E., II, Schäfer, H., Marsh, D., and Killian, J. A. (1998) Influence of lipid/peptide hydrophobic mismatch on the thickness of diacylphosphatidylcholine bilayers. A ^{2}H NMR and ESR study using designed transmembrane α-helical peptides and gramicidin A. *Biochemistry 37*, 9333–9345.
22. De Planque, M. R. R., Goormaghtigh, E., Greathouse, D. V., Koeppe, R. E., II, Kruijtzer, J. A. W., Liskamp, R. M. J., de Kruijff, B., and Killian, J. A. (2001) Sensitivity of single membrane-spanning α-helical peptides to hydrophobic mismatch with a lipid bilayer: Effects on backbone structure, orientation, and extent of membrane incorporation. *Biochemistry 40*, 5000–5010.
23. Petrache, H. I., Zuckerman, D. M., Sachs, J. N., Killian, J. A., Koeppe, R. E., II, and Woolf, T. B. (2002) Hydrophobic matching mechanism investigated by molecular dynamics simulations. *Langmuir 18*, 1340–1351.
24. Daily, A. E., Greathouse, D. V., van der Wel, P. C. A., and Koeppe, R. E., II (2008) Helical distortion in tryptophan and lysine anchored membrane-spanning α helices as a function of hydrophobic mismatch: A solid-state deuterium NMR investigation using the GALA method. *Biophys. J. 94*, 480–491.
25. Vostrikov, V. V., Grant, C. V., Daily, A. E., Opella, S. J., and Koeppe, R. E., II (2008) Comparison of "Polarization Inversion with Spin Exchange at Magic Angle" and "Geometric Analysis of Labeled Alanines" Methods for Transmembrane Helix Alignment. *J. Am. Chem. Soc. 130*, 12584–12585.
26. Demmers, J. A., van Duijn, E., Haverkamp, J., Greathouse, D. V., Koeppe, R. E., II, Heck, A. J., and Killian, J. A. (2001) Interfacial positioning and stability of transmembrane peptides in lipid bilayers studied by combining hydrogen/deuterium exchange and mass spectrometry. *J. Biol. Chem. 276*, 34501–34508.
27. Cordes, F. S., Bright, J. N., and Sansom, M. S. P. (2002) Proline-Induced Distortions of Transmembrane Helices. *J. Mol. Biol. 323*, 951–960.
28. Olivella, M., Deupi, X., Govaerts, C., and Pardo, L. (2002) Influence of the Environment in the Conformation of α-Helices Studied by Protein Database Search and Molecular Dynamics Simulations. *Biophys. J. 82*, 3207–3213.
29. Kortenaar, P. B. W., Dijk, B. G., Peeters, J. M., Raagen, B. J., Adams, P. J., and Tesser, G. I. (1986) Rapid and efficient method for the preparation of Fmoc-amino acids starting from 9-fluorenylmethanol. *Int. J. Pept. Protein Res. 27*, 398–400.
30. Greathouse, D. V., Koeppe, R. E., II, Providence, L. L., Shobana, S., and Andersen, O. S. (1999) Design and characterization of gramicidin channels. *Methods Enzymol. 294*, 525–550.
31. Turner, G. L., Hinton, J. F., Koeppe, R. E., II, Parli, J. A., and Millett, F. S. (1983) Difference in association of thallium(I) with gramicidin A and gramicidin B in trifluoroethanol determined by thallium-205 NMR. *Biochim. Biophys. Acta 756*, 133–137.
32. Davis, J. H., Jeffrey, K. R., Valic, M. I., Bloom, M., and Higgs, T. P. (1976) Quadrupolar echo deuteron magnetic resonance spectroscopy in ordered hydrocarbon chains. *Chem. Phys. Lett. 42*, 390–394.
33. Greathouse, D. V., Hinton, J. F., Kim, K. S., and Koeppe, R. E., II (1994) Gramicidin A/short-chain phospholipid dispersions: Chain length dependence of gramicidin conformation and lipid organization. *Biochemistry 33*, 4291–4299.
34. Burnett, L. J., and Muller, B. H. (1971) Deuterium quadrupole coupling constants in three solid deuterated paraffin hydrocarbons. *J. Chem. Phys. 55*, 5829–5831.
35. Strandberg, E., Özdirekcan, S., Rijkers, D. T. S., van der Wel, P. C. A., Koeppe, R. E., II, Liskamp, R. M. J., and Killian, J. A. (2004) Tilt angles of transmembrane model peptides in oriented and non-oriented lipid bilayers as determined by ^{2}H solid-state NMR. *Biophys. J. 86*, 3709–3721.
36. Manning, M., and Woody, R. W. (1991) Theoretical CD studies of polypeptide helices: Examination of important electronic and geometric factors. *Biopolymers 31*, 569–586.
37. Killian, J. A., Taylor, M. J., and Koeppe, R. E., II (1992) Orientation of the valine-1 side chain of the gramicidin transmembrane channel and implications for channel functioning. A ^{2}H NMR study. *Biochemistry 31*, 11283–11290.

38. Jude, A. R., Greathouse, D. V., Leister, M. C., and Koeppe, R. E., II (1999) Steric interactions of valines 1, 5, and 7 in [Valine 5, D-Alanine 8] gramicidin A channels. *Biophys. J. 77*, 1927–1935.
39. Page, R. C., Lee, S., Moore, J. D., Opella, S. J., and Cross, T. A. (2009) Backbone structure of a small helical integral membrane protein: A unique structural characterization. *Protein Sci. 18*, 134–146.
40. Barlow, D. J., and Thornton, J. M. (1988) Helix geometry in proteins. *J. Mol. Biol. 201*, 601–619.
41. Sankararamakrishnan, R., and Vishveshwara, S. (1992) Geometry of proline-containing α-helices in proteins. *Int. J. Pept. Protein Res. 39*, 356–363.
42. Page, R. C., Li, C., Hu, J., Gao, F. P., and Cross, T. A. (2007) Lipid bilayers: An essential environment for the understanding of membrane proteins. *Magn. Reson. Chem. 45*, S2–S11.
43. Sparr, E., Ash, W. L., Nazarov, P. V., Rijkers, D. T. S., Hemminga, M. A., Tieleman, D. P., and Killian, J. A. (2005) Self-association of transmembrane α-helices in model membranes: Importance of helix orientation and role of hydrophobic mismatch. *J. Biol. Chem. 280*, 39324–39331.
44. Özdirekcan, S., Etchebest, C., Killian, J. A., and Fuchs, P. F. J. (2007) On the Orientation of a Designed Transmembrane Peptide: Toward the Right Tilt Angle? *J. Am. Chem. Soc. 129*, 15174–15181.
45. Esteban-Martín, S., and Salgado, J. (2007) The Dynamic Orientation of Membrane-Bound Peptides: Bridging Simulations and Experiments. *Biophys. J. 93*, 4278–4288.
46. Wang, J., Denny, J., Tian, C., Kim, S., Mo, Y., Kovacs, F., Song, Z., Nishimura, K., Gan, Z., Fu, R., Quine, J. R., and Cross, T. A. (2000) Imaging membrane protein helical wheels. *J. Magn. Reson. 144*, 162–167.
47. Marassi, F. M., and Opella, S. J. (2000) A solid-state NMR index of helical membrane protein structure and topology. *J. Magn. Reson. 144*, 150–155.
48. Esteban-Martin, S., Strandberg, E., Fuertes, G., Ulrich, A. S., and Salgado, J. (2009) Influence of Whole-Body Dynamics on ^{15}N PISEMA NMR Spectra of Membrane Proteins: A Theoretical Analysis. *Biophys. J. 96*, 3233–3241.
49. Vostrikov, V. V., Grant, C. V., Opella, S. J., and Koeppe, R. E., II (2009) Orientation of Single-Span Transmembrane Peptides Investigated by Independent Solid-State NMR Methods: GALA and PISEMA. *Biophys. J. 96*, 454a.
50. Strandberg, E., Esteban-Martin, S. S. J., and Ulrich, A. S. (2009) Orientation and dynamics of peptides in membranes calculated from ^{2}H-NMR data. *Biophys. J. 96*, 3223–3232.